



# Impact of the cation distribution homogeneity on the americium oxidation state in the $U_{0.54}Pu_{0.45}Am_{0.01}O_{2-x}$ mixed oxide



Romain Vauchy<sup>a</sup>, Anne-Charlotte Robisson<sup>a,\*</sup>, Philippe M. Martin<sup>a</sup>, Renaud C. Belin<sup>a</sup>, Laurence Aufore<sup>a</sup>, Andreas C. Scheinost<sup>b</sup>, Fiqiri Hodaj<sup>c</sup>

<sup>a</sup> CEA, DEN, DEC, Centre d'études nucléaires de Cadarache, Saint Paul Lez Durance 13108, France

<sup>b</sup> Helmholtz Zentrum Dresden-Rossendorf (HZDR), Institute of Radiochemistry, P.O. Box 510119, 01314 Dresden, Germany and Rossendorf Beamline at ESRF, BP 220, F-38043 Grenoble, France

<sup>c</sup> Science et Ingénierie des Matériaux et Procédés (SIMaP, associé au CNRS UMR 5266 – UJF/INP-Grenoble), Domaine Universitaire, 1130 rue de la piscine, BP 75, 38402 Saint Martin d'Hères, France

## ARTICLE INFO

### Article history:

Received 4 June 2014

Accepted 8 September 2014

Available online 16 September 2014

## ABSTRACT

The impact of the cation distribution homogeneity of the  $U_{0.54}Pu_{0.45}Am_{0.01}O_{2-x}$  mixed oxide on the americium oxidation state was studied by coupling X-ray diffraction (XRD), electron probe micro analysis (EPMA) and X-ray absorption spectroscopy (XAS). Oxygen-hypostoichiometric Am-bearing uranium–plutonium mixed oxide pellets were fabricated by two different co-milling based processes in order to obtain different cation distribution homogeneities. The americium was generated from  $\beta^-$  decay of  $^{241}Pu$ . The XRD analysis of the obtained compounds did not reveal any structural difference between the samples. EPMA, however, revealed a high homogeneity in the cation distribution for one sample, and substantial heterogeneity of the U–Pu (so Am) distribution for the other. The difference in cation distribution was linked to a difference in Am chemistry as investigated by XAS, with Am being present at mixed +III/+IV oxidation state in the heterogeneous compound, whereas only Am(IV) was observed in the homogeneous compound. Previously reported discrepancies on Am oxidation states can hence be explained by cation distribution homogeneity effects.

© 2014 Elsevier B.V. All rights reserved.

## 1. Introduction

In the prospect of future sodium-cooled fast neutron reactors (SFR), uranium–plutonium mixed oxide fuels incorporating high amounts of plutonium are currently considered. Because of their specific neutronic spectrum, SFR will be able to burn long-lived minor actinides (MAs) such as americium [1]. Homogeneous transmutation is one possible way to reach this target by introducing small amounts (2–5%) of MAs into the  $U_{1-y}Pu_yO_{2-x}$  mixed oxide fuel. Even if some specifications are still to be discussed, general trends are already identified for such nuclear fuels. For instance, the Oxygen/Metal (O/M) ratio of the SFR's fuel will have to range from 1.94 to 2.00. This oxygen stoichiometry dictates many (or most) of the fuel properties (thermal conductivity, melting point, diffusion phenomena, ...), hence studying the O/M ratio of MA-bearing mixed oxides is relevant. The O/M ratio relies mainly on the oxidation state of the cations because metal vacancies are not expected in the uranium–plutonium mixed oxides. It is well known that, in hypostoichiometric mixed oxides  $U_{1-y}Pu_yO_{2-x}$ ,

uranium is tetravalent whereas plutonium could exhibit either fully reduced  $Pu^{3+}$  or a mixed +III/+IV valence [2–6]. Americium has been reported to be trivalent in  $(U,Pu,Am)O_{2-x}$  [7] and  $U_{1-y}Am_yO_{2-x}$  [8,9], to be of mixed valence (+III/+IV) in  $(U,Pu,Am)O_{2-x}$  [10] and  $(Pu,Am)O_{2-x}$  [11] and finally to follow the plutonium reduction behavior in  $(U,Pu,Am)O_{2-x}$  [12,13]. The americium chemistry therefore appears to be still not clearly identified within uranium–plutonium mixed oxides. Furthermore, the consequence of the cation distribution homogeneity on the americium chemistry has, to our knowledge, never been studied. Therefore, the intention of our work presented here was to investigate how the americium oxidation state is impacted by the cation homogeneity of the fuel pellet by coupling X-ray diffraction (XRD), electron probe micro analysis (EPMA) and X-ray absorption spectroscopy (XAS).

## 2. Experimental

### 2.1. Sample preparation

In this study, uranium dioxide and plutonium dioxide powders were used. The uranium dioxide powder was produced by a wet fabrication route based on the formation of ammonium diuranate

\* Corresponding author. Tel.: +33 4 42 25 73 09.

E-mail address: [anne-charlotte.robisson@cea.fr](mailto:anne-charlotte.robisson@cea.fr) (A.-C. Robisson).

(ADU) from uranyl nitrate precipitated with ammonia. The obtained particles were then atomized, dried and calcined, leading to spherical-shaped agglomerates of around 20  $\mu\text{m}$  in diameter. Plutonium dioxide powder was produced by precipitation of a plutonium nitrate solution within oxalic acid to form plutonium oxalate. The particles were heated in air at 923 K and parallelepiped-shaped  $\text{PuO}_2$  particles were obtained with an average size of 15  $\mu\text{m}$ . The americium present in the samples was due to the  $\beta^-$  decay of  $^{241}\text{Pu}$  present in the initial  $\text{PuO}_2$  powder giving a concentration Am/Metal within the samples of  $\sim 1\%$  Am in 2014.

Uranium–plutonium mixed oxide samples were obtained by mixing  $\text{UO}_2$  with  $\text{PuO}_2$  in target proportions. The obtained mixture was then micronized by co-milling with two different times (1 h and 4 h). Then, the powder was pressed into pellets ( $\sim 2$  g/pellet) at  $\sim 400$  MPa, sintered at 2023 K for 24 h under  $\text{Ar} + 5\% \text{H}_2 + \sim 1500$  vpm  $\text{H}_2\text{O}$  and slowly cooled at  $50 \text{K h}^{-1}$ . These conditions were determined according to the thermodynamic model proposed by Besmann and Lindemer [14–16] to obtain stoichiometric compounds ( $x=0$ ). The obtained pellets were free from defects (cracks, exacerbated pores...) with a high density ( $>95\%$  of the theoretical density) and the grain size was equal to 30–40  $\mu\text{m}$ . The detailed fabrication process relative to the 4 h-milled compound is described elsewhere [17]. The pellets were then annealed at 2023 K for 4 h under  $\text{Ar} + 5\% \text{H}_2 + \sim 5$  vpm  $\text{H}_2\text{O}$  and cooled as fast as possible in the considered furnace ( $300 \text{K h}^{-1}$ ) in order to obtain hypostoichiometric mixed oxides. These samples are called here “reduced samples” and referenced using the “ $\text{U}_{0.54}\text{Pu}_{0.45}\text{Am}_{0.01}\text{O}_{2-x}$ ” notation. Some of these reduced pellets

were then re-oxidized at 1173 K for 16 h under  $\text{Ar} + 5\% \text{H}_2 + \sim 24,000$  vpm  $\text{H}_2\text{O}$  leading to an O/M ratio value of  $2.000 \pm 0.001$ . These pellets are called here “stoichiometric samples” and referenced by the “ $\text{U}_{0.54}\text{Pu}_{0.45}\text{Am}_{0.01}\text{O}_{2.000}$ ” notation.

## 2.2. Apparatus and experimental technique

All XRD measurements were performed at atmospheric pressure and room temperature with a Bragg–Brentano  $\theta$ – $\theta$  Bruker D8 Advance X-ray diffractometer using copper radiation from a conventional tube source ( $K\alpha_1 + K\alpha_2$  radiation:  $\lambda = 1.5406$  and  $1.5444 \text{ \AA}$ ) at 40 kV and 40 mA on manually crushed dense pellets. The entire apparatus resides in its own custom-built nitrogen-filled glove-box dedicated to handling of actinides compounds at the LEFCA facility (CEA Cadarache). The detailed data refinement method is described in [18,19].

EPMA was performed with a Cameca SX100 device. For each microstructure, four X-ray mappings of  $1024 \times 1024$  pixels ( $1 \mu\text{m}^2$  for each pixel) were randomly selected using the displacement mode of the sample holder stage. The analysis conditions are 20 kV for electron accelerating voltage and 80 nA for beam current. Measurements were carried out on the Pu, U and O peaks without subtracting the background noise of the spectrum (continuous background) [20]. Uranium and plutonium signals were collected at the  $M\alpha$  and  $M\beta$  lines, respectively and pure standards were used:  $\text{UO}_2$  for uranium and oxygen and  $\text{PuO}_2$  for plutonium. The select counting time was about 20 ms per pixel that represented approximately 6 h of data acquisition per map. Furthermore, four concentration profiles were collected along a 500  $\mu\text{m}$  random line across each sample in order to precisely determine the cationic distribution (and its variation) within the pellets. Because of the high voltage required for its analysis (30 kV), the lack of reference material and its low concentration within the considered samples, americium was not directly analyzed by EPMA.

XAS measurements were performed at the Rossendorf Beamline (BM20) located at the European Synchrotron Radiation Facility (ESRF, Grenoble, France). Storage ring operating conditions were 6.0 GeV and 170–200 mA. A double crystal monochromator mounted with Si (111) crystals was used. XAS samples were prepared by mixing about 1 mg of material (obtained by manually crushing a dense pellet) with 20 mg of boron nitride. Samples were then pressed into a thin bar to match the dimension of the illuminating X-ray beam and then inserted into a hermetic Teflon/polyethylene sample holder. Data were collected at room temperature. This study being focused on the oxidation state of the cation, only the X-ray absorption near edge structure (XANES) part of the XAS spectra was used here. The spectra were collected at  $\text{UL}_{\text{III}}$ ,  $\text{PuL}_{\text{III}}$  and  $\text{AmL}_{\text{II}}$  edges in both transmission and fluorescence modes, using ionization chambers and a 13-elements high-purity Ge solid-state detector. More precisely, due to both vicinity of  $\text{L}_{\text{III}}$  fluorescence lines ( $L \alpha 1$  lines) of Pu and Am<sup>1</sup> and the low americium concentration on samples, Am XANES signals were consequently collected in fluorescence mode at  $\text{L}_{\text{II}}$  edge.<sup>2</sup> Since the EXAFS amplitudes are dampened by the power of 3 with photon energy  $\chi$  (the outgoing electron is a spherical wave), the slighter larger distance of  $\text{L}_{\text{II}}$  substantially reduced the influence of the Pu-EXAFS on the Am-XANES. Furthermore, the fluorescence lines can be separated more efficiently. The Darwin line width of the Si(111) monochromator crystal is about 2–3 eV, while the core-hole lifetime widening (intrinsic property of the element) is about 8–9 eV at the  $\text{AmL}_{\text{II}}$  edge. Therefore, the relatively poor resolution of the Am-XANES is dominated by an intrinsic elemental property, and

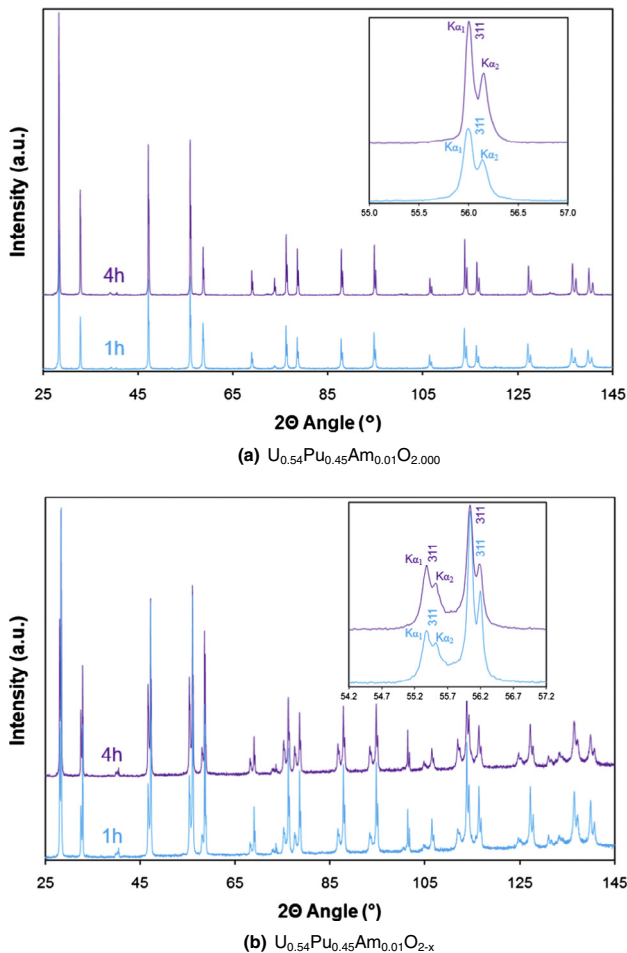


Fig. 1. X-ray diffraction patterns collected on both (a) sintered (stoichiometric) and (b) hypostoichiometric mixed oxides obtained after a 1 h- and a 4 h-co-milling.

<sup>1</sup> Am and Pu  $L \alpha 1$  lines are separated by 340 eV.

<sup>2</sup> Am and Pu  $L \beta$  lines are separated by 560 eV.

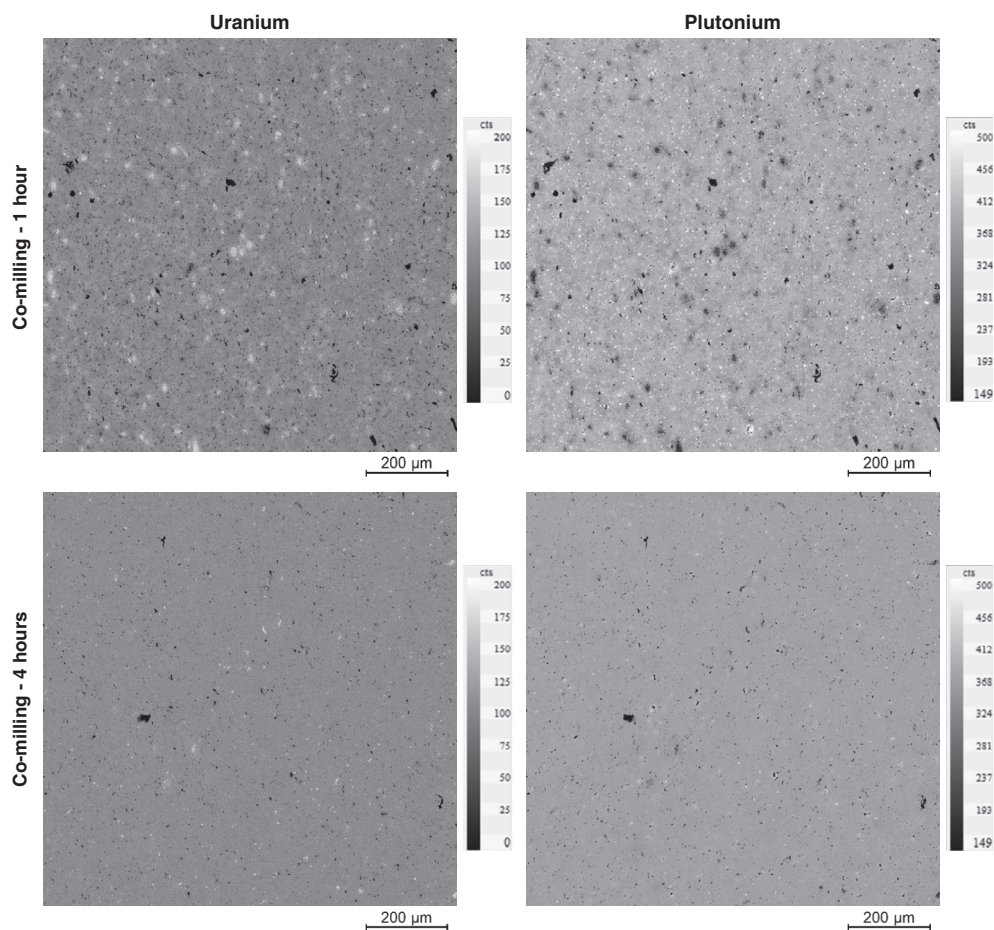


Fig. 2. EPMA X-ray mapping ( $1024 \times 1024 \mu\text{m}$ ) for the distribution of U and Pu in  $\text{U}_{0.54}\text{Pu}_{0.45}\text{Am}_{0.01}\text{O}_{2.000}$  sintered pellets obtained by co-milling for 1 h and for 4 h.

not by the Darwin width of the monochromator crystal. The repeatability of the energy as determined by the precision of the Bragg drive is even better ( $<0.5 \text{ eV}$ ), hence machine parameters are not really limiting. The energy calibration was performed using Y, Zr or Mo metallic foils located between the second and the third ionization chambers. The obtained spectra are compared to  $\text{U}_{0.90}\text{Am}_{0.10}\text{O}_{2-x}$  [9] and  $\text{AmO}_{2.00}$  [10] compounds used as Am(III) and Am(IV) references, respectively.

### 3. Results and discussion

In the prospect of ranking the samples in terms of U–Pu distribution homogeneity, XRD measurements were performed on manually crushed pellets obtained (1) after sintering at 2023 K for 24 h under Ar + 5%  $\text{H}_2$  +  $\sim 1500 \text{ vpm H}_2\text{O}$  and slowly cooled at  $50 \text{ K h}^{-1}$  [17], (2) after the reducing annealing at 2023 K for 4 h under Ar + 5%  $\text{H}_2$  +  $\sim 5 \text{ vpm H}_2\text{O}$  cooled at  $300 \text{ K h}^{-1}$  and (3) after the re-oxidizing thermal treatment at 1173 K for 16 h under Ar + 5%  $\text{H}_2$  +  $\sim 24,000 \text{ vpm H}_2\text{O}$ . The diffraction patterns (and lattice parameters) obtained after the re-oxidizing annealing (3) being identical to the one after sintering (1), only the X-ray patterns relative to the sintered and reduced samples are shown in Fig. 1. After sintering and re-oxidizing thermal treatments, the X-ray patterns were characteristic of monophasic (*f.c.c.*) samples. The corresponding lattice parameters for both milling times were equal to  $5.437 \pm 0.001 \text{ \AA}$  [17]. When determining the cell parameter by a linear interpolation between stoichiometric  $\text{UO}_2$  and  $\text{PuO}_2$  following Vegard's law, one obtains  $5.436 \text{ \AA}$  for the  $\text{U}_{0.54}\text{Pu}_{0.46}\text{O}_2$

composition [21]. Since this value is equal to the measured one, the samples were considered as stoichiometric. No influence of americium on the lattice parameter was therefore detected. After reducing annealing (2), both samples were biphasic and the lattice parameters of the two *f.c.c.* phases were equal to  $5.439 \pm 0.001 \text{ \AA}$  and  $5.496 \pm 0.001 \text{ \AA}$ , respectively [18,19]. These two phases are formed in hypostoichiometric  $\text{U}_{1-y}\text{Pu}_y\text{O}_{2-x}$  compounds (with  $y \geq 0.17$ ) because a miscibility gap exists in the  $\text{UO}_2$ – $\text{PuO}_2$ – $\text{Pu}_2\text{O}_3$  sub-system at low temperature [19,21,22]. However, these reduced samples were subjected to a spontaneous room-temperature oxidation phenomenon and both uranium and plutonium were then fully re-oxidized to +IV oxidation state when analyzed at the time of the XAS experiments [23].

In contrast to XRD, which provided no evidence for structural differences between the two fabrication processes, EPMA showed clear differences in the U–Pu distribution on the microstructural level, the 1 h co-milling sample showing a more heterogeneous cation distribution than the sample obtained from powders co-milled for 4 h (Fig. 2). This U–Pu distribution is not modified neither after the reducing annealing at 2023 K for 4 h under Ar + 5%  $\text{H}_2$  +  $\sim 5 \text{ vpm H}_2\text{O}$  (2) nor after the re-oxidizing thermal treatment at 1173 K for 16 h under Ar + 5%  $\text{H}_2$  +  $\sim 24,000 \text{ vpm H}_2\text{O}$  (3).

The concentration profiles of uranium, plutonium and oxygen species shown in Fig. 3 confirm the differences in homogeneity of cation distribution between the two mixed oxides.

The corresponding analysis of the Pu, so the Am, distribution are given in Table 1. Even if the average Pu content is identical, its standard deviation is clearly different between the two samples.

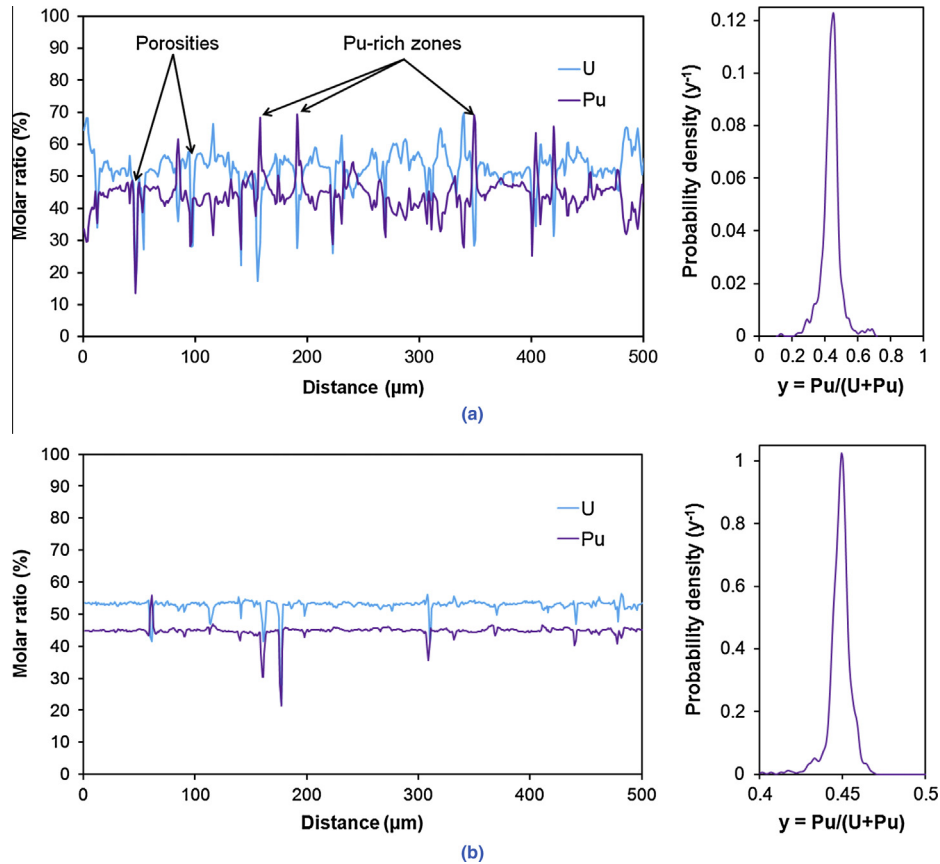


Fig. 3. EPMA quantitative elementary profiles over 500  $\mu\text{m}$  for uranium and plutonium and integrated Pu concentration along the profiles in  $\text{U}_{0.54}\text{Pu}_{0.45}\text{Am}_{0.01}\text{O}_2$  sintered pellets obtained from co-milled powders (a) for 1 h and (b) for 4 h.

Table 1

EPMA profiles results for the Pu distribution within the samples.

	Average $y = \text{Pu}/(\text{U} + \text{Pu})$	Standard deviation
Co-milling – 1 h	0.446	0.051
Co-milling – 4 h	0.452	0.005

This difference in the plutonium (so americium) distribution was an obvious evidence of  $(\text{Pu},\text{Am})\text{O}_{2-x}$  zones remaining from fabrication, even if not visible by X-ray diffraction.

The XANES results for uranium and plutonium evidenced a room temperature oxidation phenomenon since U and Pu in both

stoichiometric and reduced samples were present only at +IV oxidation state [23]. The XANES spectra of americium are given in Fig. 4 for both fabrication processes and compared to the Am(III) and Am(IV) reference compounds.

The  $\text{AmO}_{2.00}$  reference was subjected to lattice damages induced by  $\alpha$  self-irradiation, its corresponding spectra being broadened. The XANES spectra in Fig. 4 (b) overlapping the  $\text{AmO}_{2.00}$  one but exhibiting a sharper shape, the present  $\text{U}_{0.54}\text{Pu}_{0.45}\text{Am}_{0.01}\text{O}_{2.000}$  sample was used as new Am(IV) reference. The analysis of these XANES spectra made it possible to determine the amount of Am(III) and Am(IV) in each sample by linear

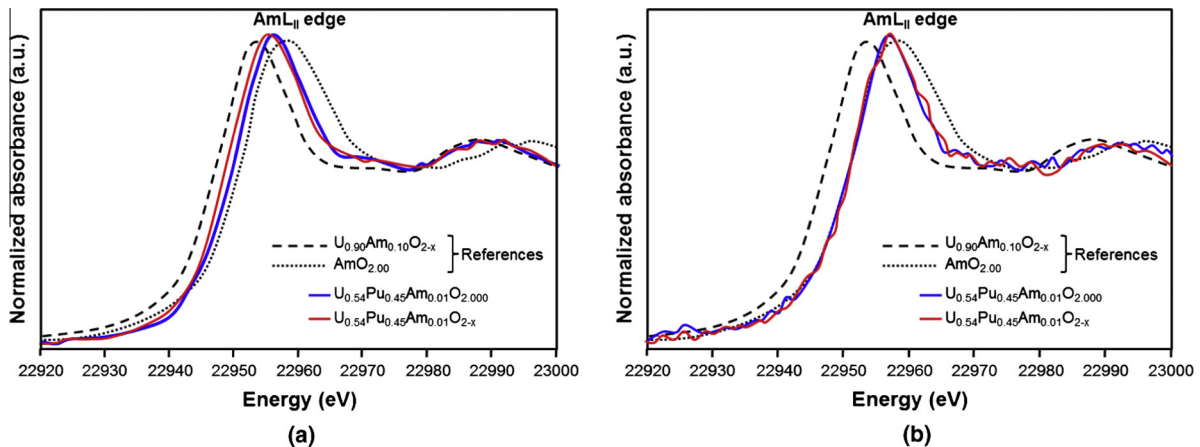


Fig. 4. XANES spectra collected in fluorescence mode at  $\text{AmL}_{\text{II}}$  edge for samples obtained from co-milled powders (a) for 1 h and (b) for 4 h.

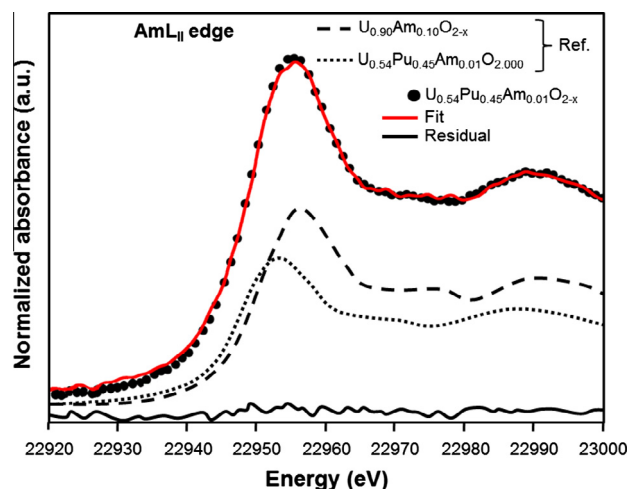


Fig. 5. Example of linear combination of the Am(III) and Am(IV) references and associated fit.

Table 2

XANES results and calculation of Am(III) and Am(IV) weight fractions for the two samples.

	wt% Am(III) Ref.	wt% Am(IV) Ref.
1 h		
Reduced	43 ± 2	57 ± 2
Stoichio.	25 ± 2	75 ± 2
4 h		
Reduced	0	100
Stoichio.	–	Used as Ref.

combination of the two reference compounds. An example is displayed in Fig. 5. The associated results are listed in Table 2.

The obtained results exhibited a clear evidence of an effect of the homogeneity of cation distribution on the americium oxidation state. The existence of local (Pu,Am) $O_{2-x}$  high concentrations made the americium to be trivalent instead of a homogeneous U–Pu distribution which led to get pure tetravalent state.

#### 4. Conclusion

The americium chemistry in uranium–plutonium mixed oxides is discussed in the literature without being able to conclude on the trivalent or tetravalent behavior of Am. The present study points

out a clear cation distribution homogeneity effect on the Am oxidation state which may explain the discrepancies between the different authors. Americium exhibits a mixed valence III/IV when the mixed oxide shows some U–Pu distribution heterogeneities. When (U,Pu,Am) $O_{2-x}$  is homogeneous, however, americium is purely tetravalent. We believe these unique results may allow a better understanding in MA-bearing uranium–plutonium mixed oxides' chemistry. The fundamental data obtained in this study will make it possible to improve the thermodynamic model describing the americium-bearing uranium–plutonium mixed oxide.

#### Acknowledgments

The authors are pleased to acknowledge Dr. J. L chelle, Dr. T. Truph mus, Dr. S. Berzati, Dr. R. Bes, I. Felines, Y. Marc and J.C. Richaud for their precious contributions to this work. The ACTINET-13 project is also to be acknowledged for allowing us to perform the XAS experiments at the ESRF facility, France.

#### References

- [1] K. Aizawa, *Prog. Nucl. Energy* 40 (2002) 349–356.
- [2] M. de Franco, J.P. Gatesoupe, *Plutonium Other Actin.* (1976) 133–143.
- [3] E. Yakub, C. Ronchi, I. Josivelski, *J. Phys.:Condens. Matt.* 18 (2006) 1227–1248.
- [4] P. Cristea, M. Stan, J.C. Ramirez, *J. Opt. Adv. Mater.* 9 (6) (2006) 1750–1756.
- [5] C. Gu neau, M. Baichi, D. Labroche, C. Chatillon, B. Sundman, *J. Nucl. Mater.* 304 (2002) 161–175.
- [6] C. Gu neau, N. Dupin, B. Sundman, C. Martial, *J. Nucl. Mater.* 419 (2011) 145–167.
- [7] M. Osaka, K. Kurosaki, S. Yamanaka, *J. Alloys Comp.* 428 (2007) 355–361.
- [8] K. Mayer, B. Kanellakopoulos, J. Naegle, L. Koch, *J. Alloys Comp.* 213–214 (1994) 456–459.
- [9] D. Prieur, P.M. Martin, F. Lebreton, T. Delahaye, D. Banerjee, A.C. Scheinost, A. Jankowiak, *J. Nucl. Mater.* 434 (2013) 7–16.
- [10] W. Bartscher, C. Sari, *J. Nucl. Mater.* 118 (1983) 220–223.
- [11] R.C. Belin, P.M. Martin, E. Gavilan, M. Reynaud, A.C. Scheinost, *Inorg. Chem.* 52 (6) (2013) 2966–2972.
- [12] M. Kato, K. Konashi, *J. Nucl. Mater.* 385 (2009) 117–121.
- [13] S. Nakamichi, M. Kato, T. Tamura, *CALPHAD* 35 (4) (2011) 648–651.
- [14] T.M. Besmann, T.B. Lindemer, Oak Ridge Technical Report, CONF-841105-59, 1984.
- [15] T.M. Besmann, T.B. Lindemer, *J. Nucl. Mater.* 130 (1985) 489–504.
- [16] T.M. Besmann, T.B. Lindemer, Oak Ridge Technical Report, CONF-851115-34, 1985.
- [17] R. Vauchy, *Ceram. Int.* 40 (7B) (2014) 10991–10999.
- [18] R. Vauchy, R.C. Belin, A.C. Robisson, F. Hodaj, *M.R.S. Proceedings, Mater. Res. Soc.* 2014 (2013) 1645.
- [19] R. Vauchy, R.C. Belin, *J. Eur. Ceram. Soc.* 34 (10) (2014) 2543–2551.
- [20] G. Oudinet, I. Munoz-Viallard, L. Aufore, *J. Nucl. Mater.* 275 (2008) 86–94.
- [21] C. Sari, U. Benedict, H. Blank, *J. Nucl. Mater.* 35 (1970) 267–277.
- [22] S. Vaudez, R.C. Belin, L. Aufore, P. Sornay, S. Grandjean, *J. Nucl. Mater.* 442 (2013) 227–234.
- [23] R. Vauchy, A.C. Robisson, P.M. Martin, R.C. Belin, A.C. Scheinost, F. Hodaj, *J. Nucl. Mater.* (submitted for publication)